Geochemical Perspectives Letters

Mobility of chromium in high-temperature crustal and upper mantle fluids

J. Huang, J. Hao, F. Huang, D.A. Sverjensky

Supplementary Information

The Supplementary Information includes:

- Theoretical Approaches
- Uncertainties in the Regression of the Experimental Data
- Fluid Models for Prediction of Cr Solutions
- Tables S-1 to S-6
- Figures S-1 and S-5
- Supplementary Information References

Theoretical approaches

To calculate the solubility of Cr in deep Earth fluids, we need the equilibrium constants of reactions involving Cr-minerals and Cr aqueous species. Therefore, the thermodynamic properties of each Cr mineral and aqueous species are essential.

For Cr-minerals we focused on eskolaite (Cr_2O_3) and picrochromite ($MgCr_2O_4$) because these are the best characterized by experimental studies and because the experimental solubilities we analyzed refer to measurements of the solubility of eskolaite. The Gibbs free energies of formation for the Cr minerals as functions of temperature and pressure were calculated using SUPCRT92b, a version of SUPCRT92 (Johnson *et al.*, 1992) based on data for minerals from Berman (1988) and Sverjensky *et al.* (1991). The thermodynamic properties of eskolaite and picrochromite are listed in Table S-1. For Cr_2O_3, the calorimetric $\Delta H^0_{f;\,Pr,Tr}$ (Klemme *et al.*, 2000) is directly used because this mineral is a pure Cr oxide endmember, its properties do not depend on those of non-Cr minerals. The heat capacities for Cr_2O_3 published by various experiments (Klemme *et al.*, 2000 and Ziemiak *et al.* 2007) showed a lambda peak transition at 305.5 K. We fitted this transition using the empirical formula from Berman and Brown (1985) (Fig. S-1). The parameters of volume were fitted based on experimental data (Dymshits *et al.*, 2016), presented in Fig. S-2.

For $MgCr_2O_4$, we also fitted the parameters of heat capacity and volume based on previous experimental data, presented as curves in Figures S-3 and S-4. Due to a lack of calorimetric experiments, the $\Delta G^0_{f;\,Pr,Tr}$ for $MgCr_2O_4$ was retrieved from the equilibrium reaction

$$MgSiO_3 + Cr_2O_3 = MgCr_2O_4 + SiO_2 \qquad \text{Eq. S-1}$$

using the thermodynamic properties of $MgSiO_3$ and SiO_2 from Berman (1988) and Cr_2O_3 obtained above (Fig. S-5).

The regression of the experimental solubility data for Cr_2O_3 was carried out to obtain values of the equilibrium constant (log K) of the $CrCl(OH)^0$ complex using EQ3, which is a theoretical code simulating water-rock equations at upper mantle conditions modified from the code published by Wolery (1983, 1992). The equation of state coefficients and standard partial molal properties for the complex $CrCl(OH)^0$ were obtained by regression using the Deep Earth Water (DEW) model to obtain the ΔG_f^0, S^0, V^0, Cp and $\omega \times 10^{-5}$ and correlation coefficients a1, a2, a3, a4, c1, and c2 of the revised Helgeson-Kirkham-Flowers equations (Helgeson *et al.*, 1981; Shock and Helgeson, 1988). In our EQ3 and DEW database, the equations of state for Cr^{3+} and Cr^{2+} were included from Hao (2016), as well as the complexes $CrCl^{2+}$, $HCrO_4^-$, CrO_4^{2-}, $Cr_2O_7^{2-}$. The thermodynamic properties of the complex $CrCl(OH)^0$ are listed in Table S-3, along with other preliminary Cr-Cl and Cr-OH complexes. Also, given are the predicted log K values extrapolated over a wide range of temperatures and pressures (Table S-4).

Uncertainties in the regression of the experimental data

The uncertainties in our values of log K obtained by regression of experimental solubilities results from experimental uncertainties and assumptions during the regression procedure. One key assumption during the regression calculations involves the $logfO_2$. In both the HCl and the KCl experiments (Watenphul *et al.*, 2014 and Klein-BenDavid *et al.*, 2011), the $logfO_2$ and pH were not directly measured. In the Deep Earth Water model, pH can be calculated by providing initial chemical compositions, mineral assemblages and the $log\ fO_2$ in the input file. However, there are suggestions about the $logfO_2$ in both experimental studies. First, the $logfO_2$ of HCl solutions (Watenphul *et al.*, 2014) was recommended as reducing but above the QFM buffer. Therefore, QFM+1 was chosen as the value of the $logfO_2$ in our models. To test the sensitivity of our log K values in response to a one-unit change of $logfO_2$, we calculated the change of log K of the complex $CrCl(OH)^0$ at 600 °C. The deviation of log K was ±0.20 and ±0.25 at 0.2 GPa and 1.0 GPa, representatively. The complex $CrCl(OH)^0$ is the dominant species between QFM and QFM+2. Second, the $logfO_2$ of KCl solutions were suggested to be near the QFM buffer. We regressed the log K of the complex $CrCl(OH)^0$ at 1000 °C and 4.0 GPa from QFM -2 to QFM +2 by fitting the points with the two highest Cl concentrations (Fig. 2), ranging from -3.31 to -3.63, with uncertainties up to +0.22. The log K of -3.53 at QFM+1 was selected for consistency with the former experiments. At the lowest Cl concentration, the predicted solubility is lower than the data, suggesting the complex $CrCl(OH)^0$ is not sufficiently important at very low Cl concentrations. There are insufficient data to characterize an additional Cr complex at those low Cl concentrations. The overall uncertainty of the regressed log K for the complex $CrCl(OH)^0$ is estimated to be ±0.3 units (Sverjensky *et al.*, 2014).

Fluid models for Prediction of Cr Solubilities

The predictions of Cr solubility in different geological environments were made using the aqueous speciation-solubility code EQ3. Fluids in three geologic settings were modelled: a mid-ocean ridge (MOR) fluid, three subduction zone fluids and a peridotitic diamond-forming fluid. For the subduction zone fluids, the predictions are applied to three types of mineral assemblages: pelitic, mafic, and ultramafic. The fluid models above were constrained by the specific mineral assemblages and conditions summarized in Table S-5.

The results of the fluid models are given as molalities of the elements and percentages of the principal aqueous species in Table S-6. The chemical compositions of fluids in different geological settings vary widely. The MOR fluid is the most dilute, because it represents altered seawater. The three subduction zone fluids have similar K concentrations. The pelitic and mafic fluids are similar in Na, Ca, Mg, Si and Fe, but lower than Al in the pelitic fluid. The pelitic fluid has the highest Cr among the subduction zone fluids because of its higher temperature but lower pressure and lower $logfO_2$ than the ultramafic fluid. The ultramafic fluid is special because it has the lowest Na, Ca, Al, Si, Fe but the highest Mg, compared with the pelitic and mafic fluids. The Cr solubility is low in the ultramafic fluid because the $logfO_2$ is buffered by the mineral assemblage antigorite, magnetite and clinochlore. The peridotitic diamond-forming fluid has the highest salinity (Cl = 8.0 mol kg^{-1}) and the highest solubilities of elements (except Mg) at 950 °C and 4.5 GPa. Therefore, the Cr solubility is remarkably high. High solubility of C exists in this fluid because of equilibrium with diamond.

The characteristics and percentage of aqueous species are various in different fluids. The complex $CrCl(OH)^0$ is the major aqueous species for Cr in every fluid. The major complexes of each other element in the MOR fluid is the simplest with only Cl ligands. In subduction zone and peridotitic fluids, silicate complexes are important, especially mixed Mg complex $Mg(SiO_2)HCO_3^+$, and Al complex $Al(OH)_3OSi(OH)_3^-$. In peridotitic fluid, aqueous organic species of methane, ethane and propane are major C species.

Supplementary Tables

Table S-1 Thermodynamic properties of Cr_2O_3 and $MgCr_2O_4$.

Mineral	ΔG_f^0 [a]	ΔH_f^0 [a]	S^0 [b]	Cp [b]	K_0 [d]	K_1 [d]	K_2 [d]	K_3 [d]
Cr_2O_3	-1,046.2[f]	-1,128.2[f]	83.8[f]	98.0[g]	139.6[g]	-501.4[g]	-1,340,000[g]	67,420,000[g]
$MgCr_2O_4$	-1,655.8[j]	-1,769.2	113.1[j]	129.0[k]	220.5[k]	-1245[k]	-2,658,000[k]	210,400,000[k]

Mineral	T_{lambda} [d]	T_{ref} [d]	l_1	l_2
Cr_2O_3	305.5[g]	298.15	-11.23 [g]	0.03676 [g]

Mineral	V^0 [c]	$v_1 \times 10^5$ [e]	$v_2 \times 10^5$ [e]	$v_3 \times 10^5$ [e]	$v_4 \times 10^8$ [e]
Cr_2O_3	29.09[h]	2.861[i]	-3.527×10^{-4} [i]	-0.05182 [i]	4.888×10^{-5} [i]
$MgCr_2O_4$	43.58[l]	1.607[m]	2.131×10^{-4} [m]	-0.05034[n]	3.513×10^{-5} [n]

[a] $kJ \cdot mole^{-1}$; [b] $J \cdot mole^{-1} \cdot K^{-1}$; [c] $cm^3 \cdot mole^{-1}$; [d]equation from Berman and Brown (1985); $Cp = k_0 + k_1 \times T^{-0.5} + k_2 \times T^{-2} + k_3 \times T^{-3} + Cp_\lambda$, when a lambda transition of the mineral at T_{lambda}, for $T_{ref} \leq T \leq T_\lambda$, $Cp_\lambda = T(l_1 + l_2 T)^2$; [e]$V = V^0[1 + v_1(T - 298) + v_2(T - 298)^2 + v_3(P - 1) + v_4(P - 1)^2]$; where T in K and P in bar; [f]calorimetric ΔH_f^0 and S from Klemme *et al*. (2000); [g]Cp parameters fitted from Klemme *et al*. (2000) and Ziemniak *et al*. (2007); [h]Holland and Powell (2011); [i]extrapolated from Dymshits *et al*. (2016); [j]retrieved from Klemme and O'Neill (1997); [k]Cp parameters fitted from Klemme *et al*. (2000) and Naylor (1944); [l]O'Neill and Dollase (1994); [m]fitted from Kaprálik (1969); [n]fitted from Nestola *et al*. (2014).

Table S-2 **(a)** log K values of $CrCl(OH)^0$ retrieved from Watenphul *et al*. (2014). Numbers in parenthesis have large uncertainties.

log K		T (°C)		
		500	600	700
P (GPa)	0.1	(-4.2)		
	0.2	(-4.1)	(-4.3)	
	0.3	(-3.9)	(-4.2)	
	0.4	(-3.6)	(-4.1)	(-4.5)
	0.5	-3.3	-3.8	-4.4
	0.6	-3.2	-3.6	-4.1
	0.7	-3.0	-3.4	-3.9
	0.8	-2.9	-3.3	-3.7
	0.9	-2.8	-3.1	-3.6
	1.0	-2.7	-3.0	-3.4

(b) Comparison of Cr_2O_3 solubility in experimental 2.249 mol kg^{-1} HCl fluids and alternate speciation models with only Cr ions, with Cr-Cl complexes, and with $CrCl(OH)^0$. Cr concentrations are in mmol kg^{-1} H_2O.

Experiment: 0.363 GPa, 500 °C; Cr = 256 mmol kg^{-1} H_2O Models:		
0.4 GPa, 500 °C	Cr solubility	Cr speciation
Only ions	1.73	Cr^{2+}(94), Cr^{3+}(6)
Cl complex	107	$CrCl_2^0$(43), $CrCl^+$(40), $CrCl_2^+$(10), $CrCl^{2+}$(6), Cr^{2+}(1)
$CrCl(OH)^0$	277	$CrCl(OH)^0$(100)

Experiment: 0.917 GPa, 600 °C; Cr = 228 mmol kg^{-1} H_2O Models:		
1.0 GPa, 600 °C	Cr solubility	Cr speciation
Only ions	3.36	Cr^{2+}(98), Cr^{3+}(2)
Cl complex	87.5	$CrCl^+$(59), $CrCl_2^0$(22), $CrCl^{2+}$(9), $CrCl_2^+$(8), Cr^{2+}(2)
$CrCl(OH)^0$	276	$CrCl(OH)^0$(100)

Table S-3 Thermodynamic properties of $CrCl(OH)^0$ and other Cr aqueous species in the DEW model from preliminary studies.

(a) Values using the units in the Deep Earth Water model.

Cr aqueous species		ΔG_f^0 [a]	ΔH_f^0 [a]	S^0 [b]	Cp [b]	V^0 [c]	$\omega \times 10^{-5}$ [a]	$a_1 \times 10$ [d]	$a_2 \times 10^{-2}$ [a]	a_3 [e]	$a_4 \times 10^{-4}$ [f]	c_1 [b]	$c_2 \times 10^{-4}$ [f]
Cr(II)	Cr^{2+}	-36,600[g]	-34,400[g]	-19.0[g]	-4.4[h]	-17.0[h]	1.35i	0.262	-9.00	8.76	-2.41	16.0	-3.93
	$CrOH^+$	-84,300[j]	-96,900	-12.1j	9.7[h]	-12.0[h]	0.73	-0.458	-4.72	8.79	-2.58	18.6	-1.06
	$CrCl^+$	-69,180[k]	-74,700	-1.74[l]	24[l]	7.8[l]	0.58	3.31	-1.13	5.79	-2.73	25.6	1.85
	$CrCl_2^0$	-100,300[k]	-115,800	7.11[l]	42.6[l]	35.4[l]	-0.038	8.38	3.69	1.74	-2.93	30.8	5.64
	$CrCl(OH)^0$	-125,200	-140,239	22.0	28.6	35.0	0.30	7.22	2.60	2.67	-2.89	29.4	4.09
Cr(III)	Cr^{3+}	-45,700[g]	-55,000[g]	-71.9[g]	-24.0[h]	-40.0[h]	2.67	-7.36	-2.80	13.4	-2.67	16.7	-7.92
	$CrOH^{2+}$	-97,200[m]	-113,800	-41.0[n]	9.5[h]	-25.7[o]	1.01	-2.67	-6.82	10.6	-2.50	27.2	-1.09
	$Cr(OH)_2^+$	-144,000[m]	-173,900	-30.1[p]	10.7[h]	-15[h]	1.01	-0.91	-5.15	9.16	-2.57	21.7	-0.86
	$CrOH_3^0$	-194,600[q]	-232,500	-0.90[q]	34[h]	3.8[h]	-0.038	2.23	-2.16	6.65	-2.69	25.7	3.89
	$CrOH_4^-$	-233,600[q]	-280,400	24.8[q]	19.3[h]	26.7[h]	1.25	7.31	2.67	2.60	-2.89	29.0	0.90
	$CrCl^{2+}$	-76,100[m]	-89,800	-45.0[p]	-2.1[r]	-17.8[l]	1.74	-1.10	-5.33	9.31	-2.56	21.0	-3.46
	$CrCl_2^+$	-106,100[m]	-122,300	-11.0[p]	-0.3[s]	6.9[l]	0.72	3.21	-1.23	5.87	-2.73	12.6	-3.10
Cr(VI)	$HCrO_4^{2-}$	-183,700[t]	-210,000[t]	46.6[t]	1.5[t]	44.9[t]	-0.963	10.7	5.90	-0.114	-3.02	15.9	-2.73
	CrO_4^{2-}	-174,800[t]	-210,930[t]	13.8[t]	-62.6[t]	19.8[t]	3.00	10.0	-6.21	1.65	-2.52	-2.86	-15.8
	$Cr_2O_7^{2-}$	-312,970[t]	-355,370 [t]	72.0[t]	-29.1[t]	72.7[t]	2.27	16.7	11.6	-4.92	-3.26	9.98	-8.96

[a] $cal \cdot mole^{-1}$; [b] $cal \cdot mole^{-1} \cdot K^{-1}$; [c] $cm^3 \cdot mole^{-1}$; [d] $cal \cdot mole^{-1} \cdot bar^{-1}$; [e] $cal \cdot K \cdot mole^{-1} \cdot bar^{-1}$; [f] $cal \cdot K \cdot mole^{-1}$. [g]Johnson and Nelson (2012); [h]calculated from the given values of S with the equations proposed by Shock *et al.*, (1997); [i]calculated from enthalpy of the complexation reaction by Dellien and Hepler (1976); [j]Slobodov *et al.* (1993); [k]calculated by assuming log β($CrCl^+$) = log β($CuCl^+$) = 0.876, log β($CrCl_{2,aq}$) = log β($CuCl_{2,aq}$) = 0.653 (Meng and Bard, 2015); [l]estimated with equations from Sverjensky *et al.* (1997); [m]calculated using the log K values recommended by Dellien *et al.* (1976); [n]ΔS_r from Baes and Mesmer (1981), originally from Postmus and King (1955); [o]Asano and Le Noble (1978); [p]calculated using ΔG_r, ΔH_r, or ΔS_r from Dellien *et al.* (1976); [q]calculated using ΔG_r and ΔS_r from Ziemniak *et al.* (1998); [r]estimated by assuming $\Delta C_{p,r} = 0$ for the reaction: $Cr^{3+} + FeCl^{2+} \rightarrow CrCl^{2+} + Fe^{3+}$; [s]estimated by assuming $\Delta C_{p,r} = 0$ for the reaction: $CrCl^{2+} + FeCl_2^+ \rightarrow CrCl_2^+ + FeCl^{2+}$; [t]Shock *et al.* (1997); [u]Accornero *et al.* (2010).

(b) Values using the SI units.

Cr aqueous species		ΔG_f^0 [a]	ΔH_f^0 [a]	S^0 [b]	Cp [b]	V^0 [c]	$\omega \times 10^{-5}$ [a]	$a_1 \times 10$ [d]	$a_2 \times 10^{-2}$ [a]	a_3 [e]	$a_4 \times 10^{-4}$ [f]	c_1 [b]	$c_2 \times 10^{-4}$ [f]
Cr(II)	Cr^{2+}	-153.1	-143.9	-79.5	-18.4	-17.0	5.65	1.10	-37.7	36.7	-10.1	66.9	-16.4
	$CrOH^+$	-352.7	-405.4	-50.6	40.6	-12.0	3.05	-1.92	-19.7	36.8	-10.8	77.8	-4.40
	$CrCl^+$	-289.4	-312.5	-7.28	100	7.80	2.43	13.9	-4.70	24.2	-11.4	107	7.70
	$CrCl_2^0$	-419.7	-484.5	29.8	178	35.4	-0.160	35.1	15.4	7.30	-12.3	129	23.6
	$CrCl(OH)^0$	-523.8	-586.8	92.1	120	35.0	1.26	30.2	10.9	11.2	-12.1	123	17.1
Cr(III)	Cr^{3+}	-191.2	-230.1	-301	-100	-40.0	11.2	-30.8	-11.7	56.1	-11.2	69.9	-33.1
	$CrOH^{2+}$	-406.7	-476.1	-172	39.8	-25.7	4.23	-11.2	-28.5	44.4	-10.5	114	-4.60
	$Cr(OH)_2^+$	-602.5	-727.6	-126	44.8	-15.0	4.23	-3.81	-21.5	38.3	-10.8	90.8	-3.60
	$CrOH_3^0$	-814.2	-972.8	-3.77	142	3.80	-0.160	9.33	-9.00	27.8	-11.3	108	16.3
	$CrOH_4^-$	-977.4	-1173	104	80.8	26.7	5.23	30.6	11.2	10.9	-12.1	121	3.80
	$CrCl^{2+}$	-318.4	-375.7	-188	-8.79	-17.8	7.28	-4.60	-22.3	39.0	-10.7	87.9	-14.5
	$CrCl_2^+$	-443.9	-511.7	-46.0	-1.26	6.90	3.01	13.4	-5.10	24.6	-11.4	52.7	-13.0
Cr(VI)	$HCrO_4^{2-}$	-768.6	-878.6	195	6.28	44.9	-4.03	44.8	24.7	-0.500	-12.6	66.5	-11.4
	CrO_4^{2-}	-731.4	-882.5	57.7	-262	19.8	12.6	41.8	-26.0	6.90	-10.5	-12.0	-66.1
	$Cr_2O_7^{2-}$	-1310	-1487	301	-122	72.7	9.50	69.9	48.5	-20.6	-13.6	41.8	-37.5

[a] $kJ \cdot mole^{-1}$; [b] $J \cdot mole^{-1} \cdot K^{-1}$; [c] $\times 10^{-6}\ m^3 \cdot mole^{-1}$; [d] $\times 10^{-5}\ J \cdot mole^{-1} \cdot Pa^{-1}$; [e] $\times 10^{-5}\ J \cdot K \cdot mole^{-1} \cdot Pa^{-1}$; [f] $J \cdot K \cdot mole^{-1}$.

Table S-4 Predicted log K of dissociation reaction for $CrCl(OH)^0$.

log K		P (GPa)						
		0.5	1.0	2.0	3.0	4.0	5.0	6.0
T (°C)	300	-1.9	-1.6	-1.5	-1.5	-1.5	-1.5	-1.4
	350	-2.2	-1.9	-1.7	-1.6	-1.6	-1.6	-1.5
	400	-2.5	-2.1	-1.8	-1.8	-1.7	-1.7	-1.6
	450	-2.8	-2.3	-2.0	-1.9	-1.9	-1.8	-1.8
	500	-3.1	-2.5	-2.2	-2.1	-2.0	-2.0	-1.9
	550	-3.4	-2.8	-2.4	-2.2	-2.2	-2.1	-2.0
	600	-3.8	-3.0	-2.6	-2.4	-2.3	-2.2	-2.2
	650	-4.1	-3.3	-2.8	-2.6	-2.5	-2.4	-2.3
	700	-4.5	-3.5	-2.9	-2.7	-2.6	-2.5	-2.5
	750	-4.9	-3.8	-3.1	-2.9	-2.8	-2.7	-2.6
	800	-5.3	-4.0	-3.3	-3.1	-2.9	-2.8	-2.7
	850	-5.7	-4.3	-3.5	-3.2	-3.1	-3.0	-2.9
	900	-6.1	-4.5	-3.7	-3.4	-3.2	-3.1	-3.0
	950	-6.6	-4.8	-3.8	-3.5	-3.4	-3.3	-3.2
	1000	-7.0	-5.0	-4.0	-3.7	-3.5	-3.4	-3.3
	1050	-7.4	-5.3	-4.2	-3.9	-3.7	-3.6	-3.5
	1100	-7.8	-5.5	-4.4	-4.0	-3.8	-3.7	-3.6

Table S-5 Characteristics of model crustal and upper mantle fluids for predicting Cr solubilities.

Type of fluids	T	P	$logfO_2$	Cl	Mineral assemblage
Mid-Ocean Ridge	350	Psat 0.017	-25.2 (Pa)	0.49	talc, clinochlore, quartz, magnetite, and eskolaite
Pelitic schist	650	1.0	QFM	0.5	plagioclase(ss): albite (53), anorthite (47); biotite(ss): phlogopite (88), annite (12); muscovite, kyanite, quartz, and eskolaite
Mafic eclogitic	570	2.0	QFM-1	0.5	garnet(ss): pyrope (12), almandine (63), grossular (25); omphacite(ss): diopside (32), hedenbergite (26), jadeite (42); quartz, and eskolaite
Ultramafic antigorite	630	2.0	QFM+2	0.6	antigorite, magnetite, clinochlore, and picrochromite
Peridotitic diamond	950	4.5	QFM-4	8.0	garnet(ss): pyrope (69), almandine (15), grossular (16); olivine(ss):forsterite (92), fayalite (8); orthopyroxene(ss): enstatite-or (91), ferrosilite (9); phlogopite, diamond, and picrochromite

Temperature in °C, pressure in GPa and Cl in $mol\ kg^{-1}$.

Source of fluid models: mid-ocean ridge mineral assemblage based on a speciation solubility model of the chemical analysis reported by Von Damm (1990); pelitic mineral assemblage represents a hypothetical pelitic schist; mafic mineral assemblage based on Viete *et al.* (2018); ultramafic mineral assemblage from Debret and Sverjensky (2017); peridotitic mineral assemblage from Huang (2017).

Table S-6 Solubilities (**a – c**) and speciation (**d – f**) of model crustal and upper mantle fluids. The unit of solubilities of elements is mmol kg^{-1} H_2O. The numbers in parentheses represent the percentages of each aqueous species of a given chemical element.

(a)	350 °C, Psat (0.017 GPa)
ELEMENT	Mid-ocean ridge
Na	$4.3*10^{-1}$
K	$2.5*10^{-2}$
Ca	$1.0*10^{-2}$
Mg	$2.6*10^{-3}$
Al	$8.8*10^{-7}$
Si	$1.3*10^{-2}$
Fe	$1.8*10^{-3}$
Zn	$1.1*10^{-4}$
Pb	$4.8*10^{-7}$
S	$2.3*10^{-3}$
C	$4.7*10^{-3}$
Cr	2.8*10-6
log$f$O2 (Pa)	-25.2
ΔQFM	+1.8
pH	4.79
a_{H_2O}	0.99

(b)	650 °C, 1.0 GPa	570 °C, 2.0 GPa	630°C, 2.0 GPa
ELEMENT	Pelitic Schist	Eclogitic mafic	Antigorite ultramafic
Na	$3.5*10^{-1}$	$4.1*10^{-1}$	$1.4*10^{-1}$
K	$7.7*10^{-2}$	$1.0*10^{-1}$	$1.0*10^{-1}$
Ca	$1.9*10^{-2}$	$1.9*10^{-2}$	$1.0*10^{-3}$
Mg	$4.5*10^{-2}$	$3.0*10^{-2}$	$6.6*10^{-1}$
Al	$9.1*10^{-3}$	$2.5*10^{-2}$	$5.1*10^{-4}$
Si	$5.7*10^{-1}$	$5.3*10^{-1}$	$4.5*10^{-1}$
Fe	$6.5*10^{-2}$	$7.0*10^{-2}$	$3.5*10^{-2}$
C	1.0	1.0	1.0
Cr	$1.1*10^{-4}$	$3.9*10^{-5}$	$9.8*10^{-6}$
log$f$O2 (Pa)	-12.3	-15.3	-8.7
ΔQFM	0	-1	+2
pH	4.83	4.91	4.50
a_{H_2O}	0.98	0.98	0.98

(c)	950 °C, 4.5 GPa
ELEMENT	Peridotitic diamond-forming
Na	2.5
K	4.7
Ca	$6.1*10^{-1}$
Mg	$2.3*10^{-1}$
Al	$9.9*10^{-2}$
Si	1.3
Fe	$2.7*10^{-1}$
C	$7.4*10^{2}$
Cr	$6.8*10^{-2}$
log$f$O2 (Pa)	-7.6
ΔQFM	-4
pH	4.64
a_{H_2O}	0.76

(d)	350 °C, Psat (0.017 GPa)
ELEMENT	**Mid-ocean ridge**
Na	$NaCl^0$(55), Na^+(45)
K	K^+(74), KCl^0(26)
Ca	$CaCl_2^0$(60), $CaCl^+$(24), Ca^{2+}(16)
Mg	$MgCl^+$(92), Mg^{2+}(8)
Al	$AlCl_4^-$(79), $AlCl_3^0$(18), $AlOH_4^-$(3)
Si	$SiO_2(aq)$(100)
Fe	$FeCl_2^0$(98), $FeCl^+$(2)
Zn	$ZnCl_4^{2-}$(87), $ZnCl^+$(7), $ZnCl_2^0$(6)
Pb	$PbCl_2^0$(46), $PbCl_3^-$(40), $PbCl_4^{2-}$(11), $PbCl^+$(3)
S	$H_2S(aq)$(100)
C	$CO_2(aq)$(100)
Cr	$CrCl(OH)^0$(100)
log$f$O$_2$	-25.2 Pa
ΔQFM	+1.8
pH	4.79
a_{H_2O}	0.99

(e)	650 °C, 1.0 GPa	570 °C, 2.0 GPa	630°C, 2.0 GPa
ELEMENT	**Pelitic Schist**	**Eclogitic mafic**	**Antigorite ultramafic**
Na	Na^+(85), $NaCl^0$(15)	Na^+(85), $NaHCO_3^0$(11), $NaCl^0$(4)	Na^+(85), $NaHCO_3^0$(8), $NaCl^0$(6)
K	K^+(89), KCl^0(11)	K^+(96), KCl^0(3), KOH^0(1)	K^+(95), KCl^0(5)
Ca	$Ca(H_3SiO_4)^+$(87), $CaCl^+$(11), $Ca(HCO_3)^+$(1)	$Ca(H_3SiO_4)^+$(67), $Ca(HCO_3)^+$(21), $Ca(HCOO)^+$(6), $CaCl^+$(5), Ca^{2+}(1)	$Ca(HCO_3)^+$(56), Ca$(H_3SiO_4)^+$(23), $CaCl^+$(18), Ca^{2+}(2)
Mg	$Mg(OH)_2^0$(96), $Mg(SiO_2)HCO_3^+$(4),	$Mg(SiO_2)HCO_3^+$(61), $Mg(OH)_2^0$(39)	$Mg(SiO_2)HCO_3^+$(52), $Mg(OH)_2^0$(48)
Al	$Al(OH)_3OSi(OH)_3^-$(84), AlO_2^-(9), $HAlO_2(aq)$(7)	$Al(OH)_3OSi(OH)_3^-$ (94), AlO_2^-(5), $HAlO_2(aq)$(1)	$Al(OH)_3OSi(OH)_3^-$ (66), AlO_2^-(19), $HAlO_2(aq)$(15)
Si	$SiO_2(aq)$(50), $Si_2O_4(aq)$(35), $Fe(H_3SiO_4)^+$(11), Ca$(H_3SiO_4)^+$(3), $Al(OH)_3OSi(OH)_3^-$ (1)	$SiO_2(aq)$(50), $Si_2O_4(aq)$(27), $Fe(H_3SiO_4)^+$(10), $Al(OH)_3OSi(OH)_3^-$(5), $Mg(SiO_2)HCO_3^+$(3), $H_3SiO_4^-$(2), Ca$(H_3SiO_4)^+$(2)	$Mg(SiO_2)HCO_3^+$(76), $SiO_2(aq)$(15), $Fe(H_3SiO_4)^+$(7), $Si_2O_4(aq)$(2)
Fe	$Fe(H_3SiO_4)^+$(99), $FeCl_2^0$(1)	$Fe(H_3SiO_4)^+$(73), $Fe(HCOO)^+$(27)	$Fe(H_3SiO_4)^+$(92), $FeCl_2^0$(7), $Fe(HCOO)^+$(1)
C	$H_2CO_3(aq)$(92), $CO_2(aq)$(8)	$CH_4(aq)$(72), $CO_2(aq)$(18), $NaHCO_3^0$(4), $Fe(HCOO)^+$(2), $Mg(SiO_2)HCO_3^+$(2), $HCOO^-$(1), HCO_3^-(1)	$CO_2(aq)$(64), $Mg(SiO_2)HCO_3^+$(34), $NaHCO_3^0$(1),
Cr	$CrCl(OH)^0$(100)	$CrCl(OH)^0$(88), $Cr(OH)_4^-$ (7), $Cr(OH)_3^0$(5)	$CrCl(OH)^0$(87), $Cr(OH)_4^-$ (7), $Cr(OH)_3^0$(6)
log$f$O$_2$	-12.3 Pa	-15.3 Pa	-8.7 Pa
ΔQFM	0	-1	+2
pH	4.83	4.91	4.50
a_{H_2O}	0.98	0.98	0.98

(f)	950 °C, 4.5 GPa
ELEMENT	**Peridotitic diamond-forming**
Na	Na^+(75), $NaCl^0$(17), $NaOH^0$(5), $NaHCO_3^0$(3)
K	K^+(56), KCl^0(41), KOH^0(4)
Ca	$Ca(HSiO)_3^+$(70), $CaCl^+$(26), $CaCl_2^0$(3)
Mg	$Mg(SiO_2)HCO_3^+$(98), $MgCl^+$(2)
Al	$Al(OH)_3OSi(OH)_3^-$(84), $HAlO_2(aq)$(8), AlO_2^-(8)
	$Ca(HSiO)_3^+$(34), $SiO_2(aq)$(31), $Mg(SiO_2)HCO_3^+$(18), $AlO_2(SiO_2)^-$(7), $HSiO_3^-$(6),
Si	$Fe(HSiO_3)^+$(3), $Si_2O_4(aq)$(3)
Fe	$FeCl_2^0$(82), $Fe(HSiO_3)^+$(12), $Fe(HCO_3)^+$(6)
C	$CH_4(aq)$(58), ethane(aq)(27), propane(aq)(12), ethanol(aq)(4)
Cr	$CrCl(OH)^0$(100)
logfO_2	-7.6 Pa
ΔQFM	-4
pH	4.64
a_{H_2O}	0.76

Supplementary Figures

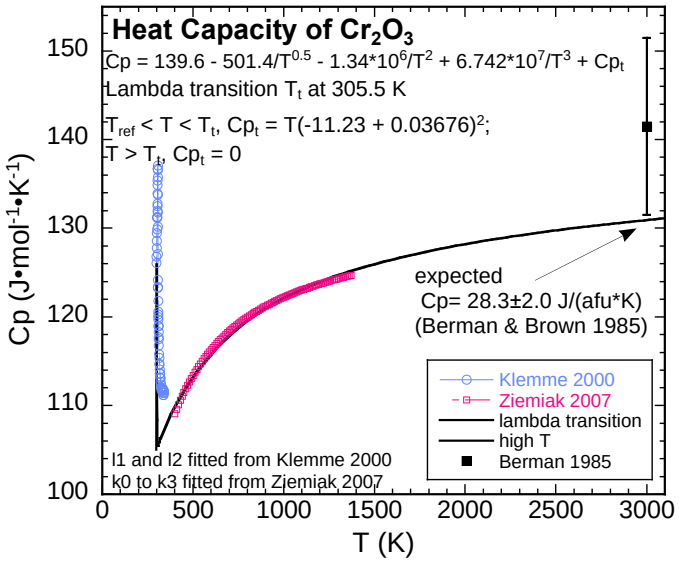

Figure S-1 Fitting of heat capacity for Cr_2O_3 at 10^5 Pa, from 273.15 K to 3000 K, based on experimental data from Klemme *et al*. (2000) and Ziemiak *et al*. (2007).

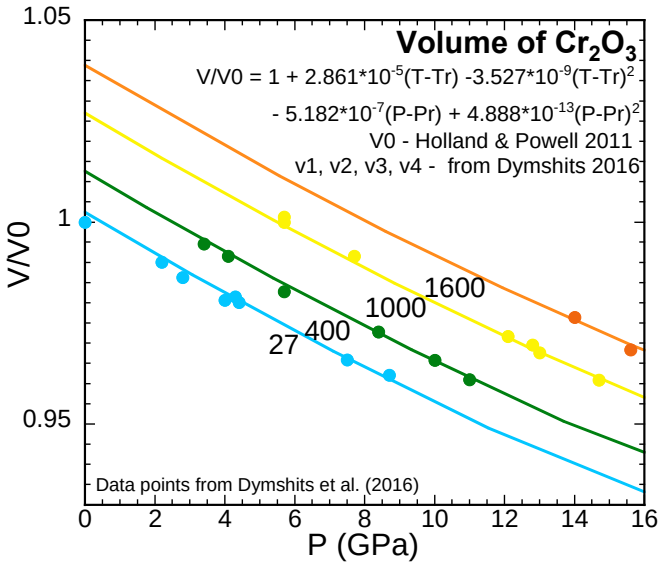

Figure S-2 Fitting of volume for Cr_2O_3 at pressures from 10^5 Pa to 15 GPa, and temperatures from 27 °C to 1600 °C, based on experimental data from Dymshits *et al.* (2016).

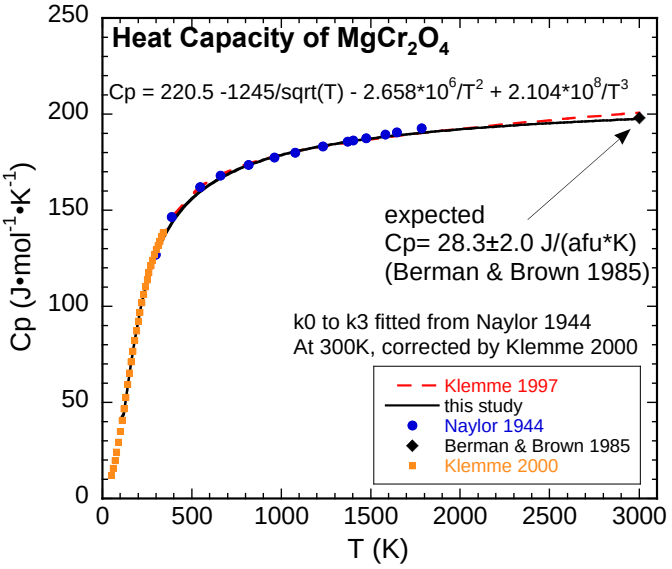

Figure S-3 Fitting of heat capacity for $MgCr_2O_4$ at 10^5 Pa from 0 K to 3000 K, based on experimental data from Klemme and O'Neill (1997), Klemme *et al*. (2000), and Naylor (1944).

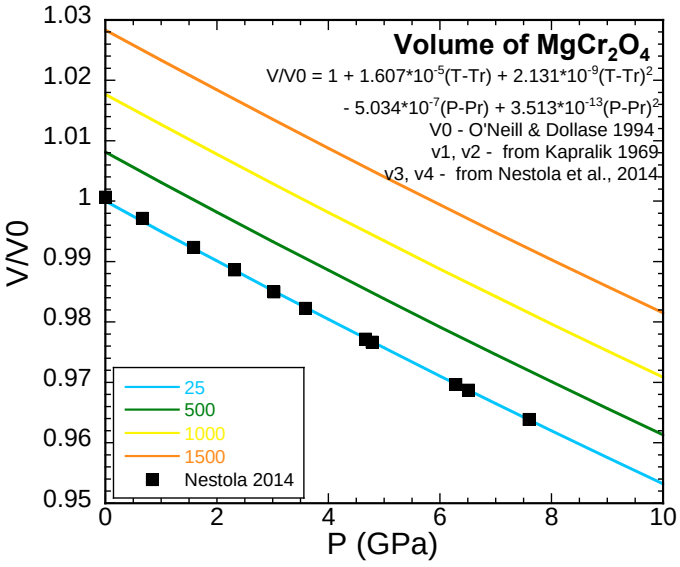

Figure S-4 Fitting of volume for $MgCr_2O_4$ at pressures from 10^5 Pa to 10 GPa, and temperatures from 25 °C to 1500 °C, based on experimental data from Kaprálik (1969) and Nestola *et al*. (2014).

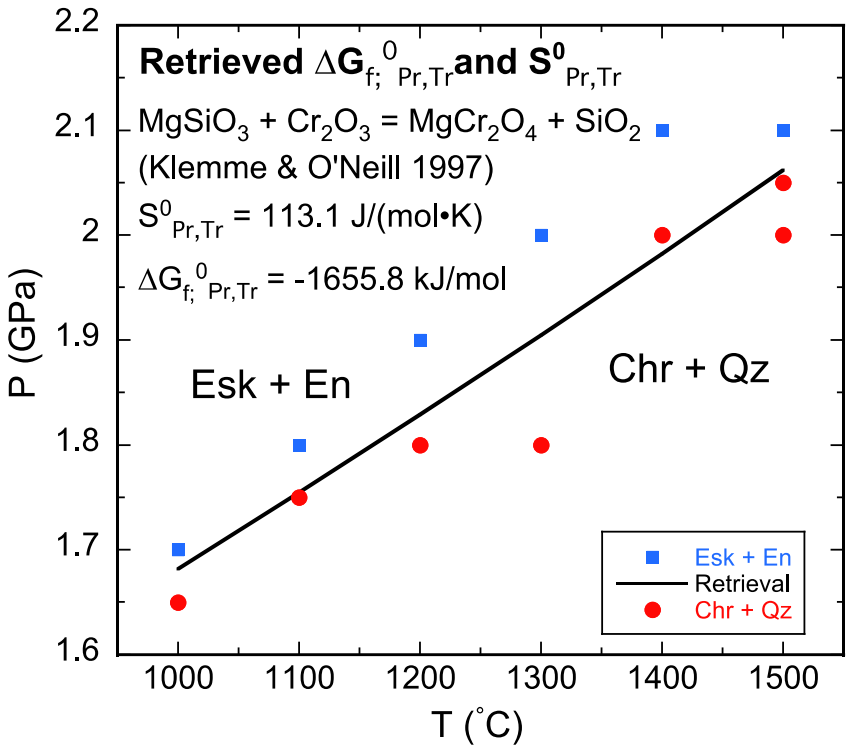

Figure S-5 Retrieval of Gibbs free energy of formation and entropy at 25 °C, 10^5 Pa for $MgCr_2O_4$, based on experimental data from Klemme and O'Neill (1997).

Supplementary Information References

Accornero, M., Marini, L., Lelli, M. (2010) Prediction of the thermodynamic properties of metal-chromate aqueous complexes to high temperatures and pressures and implications for the speciation of hexavalent chromium in some natural waters. *Applied Geochemistry* 25, 242–260.

Asano, T., Le Noble, W.J. (1976) Activation and Reaction Volumes in Solution. *Chemical Reviews* 78, 407–489.

Baes Jr, C.F., Mesmer, R.E. (1981) Thermodynamics of cation hydrolysis. *Am. J. Sci.;(United States)* 281.

Berman, R.G. (1988) Internally-Consistent Thermodynamic Data for Minerals in the System Na2O-K2O-CaO-MgO-FeO-Fe2O3-Al2O3-SiO2-TiO2-H2O-CO2. *Journal of Petrology* 29, 445–522.

Berman, R.G., Brown, T.H. (1985) Heat capacity of minerals in the system Na2O-K2O-CaO-MgO-FeO-Fe2O3-Al2O3-SiO2-TiO2-H2O-CO2: representation, estimation, and high temperature extrapolation. *Contributions to Mineralogy and Petrology* 89, 168–183.

Debret, B., Sverjensky, D.A. (2017) Highly oxidising fluids generated during serpentinite breakdown in subduction zones. *Scientific Reports* 7.

Dellien, I., Hall, F.M., Hepler, L.G (1976) Chromium, molybdenum, and tungsten: thermodynamic properties, chemical equilibria, and standard potentials. *Chemical Reviews* 76, 283–310.

Dellien, I., Hepler, L.G. (1976) Enthalpies of formation of Cr 3+ (aq) and the inner sphere complexes CrF 2+ (aq), CrCl 2+ (aq), CrBr 2+ (aq), and CrSO 4+ (aq). *Canadian Journal of Chemistry* 54, 1383–1387.

Dymshits, A., Iagher, L., Etgar, L. (2016) Parameters influencing the growth of ZnO nanowires as efficient low temperature flexible perovskite-based solar cells. *Materials* 9, 60.

Hao, J. (2016) Geochemical signatures of weathering and surface water chemistry in the late Archean. PhD thesis, Johns Hopkins University, 248 pp.

Huang, F. (2017) Evolution of aqueous fluids, hydrocarbons, and diamond formation in the upper mantle. PhD thesis, Johns Hopkins University, 207 pp.

Helgeson, H.C., Kirkham, D.H., Flowers, G.C. (1981) Theoretical prediction of the thermodynamic behavior of aqueous electrolytes at high pressures and temperatures: IV. Calculation of activity coefficients, osmotic coefficients, and apparent molal and standard and relative partial molal properties to 600oC. *American Journal of Science* 281, 1249–1516.

Holland, T.J.B., Powell, R. (2011) An improved and extended internally consistent thermodynamic dataset for phases of petrological interest, involving a new equation of state for solids. *Journal of Metamorphic Geology* 29, 333–383.

Johnson, D.A., Nelson, P.G. (2012) Improvements in estimated entropies and related thermodynamic data for aqueous metal ions. *Inorganic Chemistry* 51, 6116–6128.

Johnson, J.W., Oelkers, E.H., Helgeson, H.C. (1992) SUPCRT92: A software package for calculating the standard molal thermodynamic properties of minerals, gases, aqueous species, and reactions from 1 to 5000 bar and 0 to 1000°C. *Computers and Geosciences* 18, 899–947.

Kaprálik, I. (1969) Thermal Expansion of Spinels MgCr2O4, MgAl2O4 and MgFe2O4. *Chemical Papers* 23, 665–670.

Klein-BenDavid Ofra, O., Pettke, T., Kessel, R. (2011) Chromium mobility in hydrous fluids at upper mantle conditions. *Lithos* 125, 122–130.

Klemme, S., O'Neill, H.S.C. (1997) The reaction MgCr2O4+ SiO2= Cr2O3+ MgSiO3and the free energy of formation of magnesiochromite (MgCr2O4). *Contributions to Mineralogy and Petrology* 130, 59–65.

Klemme, S., O'Neill, H.S.C., Schnelle, W., Gmelin, E. (2000) The heat capacity of MgCr2O4, FeCr2O4, and Cr2O3at low temperatures and derived thermodynamic properties. *American Mineralogist* 85, 1686–1693.

Meng, Y., Bard, A.J. (2015) Measurement of Temperature-Dependent Stability Constants of Cu(I) and Cu(II) Chloride Complexes by Voltammetry at a Pt Ultramicroelectrode. *Analytical Chemistry* 87, 3498–3504.

Naylor, B.F. (1944) High-Temperature Heat Contents Of Ferrous and Magnesium Chromites. *Industrial and Engineering Chemistry* 36, 933–934.

Nestola, F., Periotto, B., Andreozzi, G.B., Bruschini, E., Bosi, F. (2014) Pressure-volume equation of state for chromite and magnesiochromite: A single-crystal X-ray diffraction investigation. *American Mineralogist* 99, 1248–1253.

O'Neill, H.S.C., Dollase, W.A. (1994) Crystal Structures and Cation Distributions in Simple Spinels from Powder XRD Structural Refinements : and the Temperature Dependence of the Cation Distribution in ZnAl2O4. *Physics and Chemistry of Minerals* 20, 541–555.

Postmus, C., King, E.L. (2005) The Equilibria in Acidic Solutions of Chromium(III) Ion and Thiocyanate Ion. *The Journal of Physical Chemistry* 59, 1208–1216.

Shock, E.L., Sassani, D.C., Willis, M., Sverjensky, D.A. (1997) Inorganic species in geologic fluids: Correlations among standard molal thermodynamic properties of aqueous ions and hydroxide complexes. *Geochimica et Cosmochimica Acta* 61, 907–950.

Slobodov, A.A., Kritskii, A. V., Zarembo, V.I., V., P.L. (1993) THERMODYNAMIC ANALYSIS OF THE CHEMICAL-REACTIONS OF CHROMIUM WITH AQUEOUS-SOLUTIONS. *Russian Journal of Applied Chemistry* 66, 39–48.

Sverjensky, D.A., Hemley, J.J., D'angelo, W.M. (1991) Thermodynamic assessment of hydrothermal alkali feldspar-mica-aluminosilicate equilibria. *Geochimica et Cosmochimica Acta* 55, 989–1004.

Sverjensky, D.A., Shock, E.L., Helgeson, H.C. (1997) Prediction of the thermodynamic properties of aqueous metal complexes to 1000°C and 5 kb. *Geochimica et Cosmochimica Acta* 61, 1359–1412.

Sverjensky, D.A., Harrison, B., Azzolini, D. (2014). Water in the deep Earth: the dielectric constant and the solubilities of quartz and corundum to 60 kb and 1200 C. *Geochimica et Cosmochimica Acta*, *129*, 125-145.

Viete, D.R., Hacker, B.R., Allen, M.B., Seward, G.G., Tobin, M.J., Kelley, C.S., Cinque, G., Duckworth, A.R. (2018) Metamorphic records of multiple seismic cycles during subduction. *Science Advance* 4, eaaq0234.

Von Damm, K.L. (1990) Seafloor hydrothermal activity: black smoker chemistry and chimneys. *Annual Review of Earth and Planetary Sciences* 18, 173-204.

Watenphul, A., Schmidt, C., Jahn, S. (2014) Cr(III) solubility in aqueous fluids at high pressures and temperatures. *Geochimica et Cosmochimica Acta* 126, 212–227.

Ziemniak, S.E., Anovitz, L.M., Castelli, R.A., Porter, W.D. (2007) Thermodynamics of Cr2O3, FeCr2O4, ZnCr2O4, and CoCr2O4. *Journal of Chemical Thermodynamics* 39, 1474–1492.

Ziemniak, S.E., Jones, M.E., Combs, K.E.S. (1998) Solubility and phase behavior of Cr(III) oxides in alkaline media at elevated temperatures. *Journal of Solution Chemistry* 27, 33–66.